# Accretion-Induced Lithium Line Enhancements in Classical T Tauri Stars: RW Aur

N.M. Stout-Batalha and C.C. Batalha

Observatório Nacional/CNPq, Rua General José Cristino, 77, Rio de Janeiro, RJ 20920, Brasil

natalie@on.br, celso@on.br

G.S. Basri

University of California, Berkeley, CA 94720

basri@soleil.berkeley.edu

Received _____; accepted _____

**ABSTRACT**

It is widely accepted that much of the stochastic variability of T Tauri stars is due to accretion by a circumstellar disk. The emission line spectrum as well as the excess continuum emission are common probes of this process. In this communication, we present additional probes of the circumstellar environment in the form of resonance lines of low ionization potential elements. Using a set of 14 high resolution echelle observations of the classical T Tauri star (CTTS), RW Aur, taken between 1986 and 1996, we carefully measure the continuum veiling at each epoch by comparing more than 500 absorption lines with those of an appropriate template. This allows us to accurately subtract out the continuum emission and to recover the underlying photospheric spectrum. In doing so, we find that selected photospheric lines are enhanced by the accretion process, namely the resonance lines of LiI and KI. A resonance line of TiI and a low excitation potential line of CaI also show weak enhancements. Simple slab models and computed line bisectors lead us to propose that these line enhancements are markers of cool gas at the beginning of the accretion flow which provides an additional source of line opacity. These results suggest that published values of surface lithium abundances of classical T Tauri stars are likely to be overestimated. This would account for the various reports of surface lithium abundances in excess of meteoritic values among the extreme CTTS. Computing LTE lithium abundances of RW Aur in a low and then high accretion state yields abundances which vary by one order of magnitude. The low accretion state lithium abundance is consistent with theoretical predictions for a star of this age and mass while the high accretion state spectrum yields a super-meteoritic lithium abundance.

*Subject headings:* accretion, accretion disks ··· stars: abundances ··· stars: individual (RW Aur) ··· stars: late-type ··· stars: pre-main sequence ···

## 1. Introduction

When an overabundance of lithium (a factor of 100 greater than in the Sun) was first detected in a small sample of T Tauri stars, it was speculated that either the circumstellar environment of these stars furnishes fresh lithium, or that the stars are too young to have undergone appreciable lithium destruction (Bonsack & Greenstein 1960, Zappala 1972). The latter argument is supported by the meteoritic lithium abundances which, at $\epsilon(N_{Li}) = 3.3$ (Nichiporuk & Moore 1974), are also found to be several orders of magnitude greater than that of the Sun at $\epsilon(N_{Li}) = 1.16 \pm 0.1$ (Anders & Grevesse 1989). Bodenheimer (1965) laid out the physics for the destruction of lithium in late-type stars whereby surface lithium is carried via convection to interior regions hotter than $\sim 2.4 \times 10^6$ K. At such high temperatures, lithium is destroyed in (p,$\alpha$) reactions. The idea that surface lithium abundances could be used as age indicators became widespread. The question became: exactly how and when does lithium depletion take place?

Early theoretical work, such as that of Bodenheimer, predicted that the surface lithium depletion would be a function of stellar mass and age. However, observations of coeval populations in young open clusters revealed that the relation would not be so simple. Duncan & Jones (1983), in a study of F, G, and K-type stars in the Pleiades cluster ($\sim$ 100 Myr), found a spread in the lithium abundance (as much as 1.0 dex) for a given mass. Since that time, extensive studies of open cluster stars of varying ages and masses have emerged in the literature. From studies of IC 2602 at 30 Myr (Randich et al. 1996), IC 4665 at $\sim$ 50 Myr (Martín & Montes 1997), the $\alpha$ Persei cluster at 70 Myr (Balachandran, Lambert, & Stauffer 1988, Randich et al. 1998, Basri & Martin 1999), the Pleiades at 120 Myr (Soderblom et al. 1993b, García-Lopez, Rebolo, & Martín 1994, Jones et al. 1996, Basri, Marcy, & Graham 1996, Stauffer et al. 1998), NGC 2516 at 150 Myr (Jeffries, James, & Thurston 1998), NGC 6475 at 220 Myr (James & Jeffries 1997), NGC 1039 at 250 Myr (Jones et al. 1997), the Hyades at 700 Myr (Cayrel et al. 1984, Thorburn et al. 1993, Soderblom et al. 1995), the Praesepe cluster at 700 Myr (Soderblom et al. 1993a), and the much older cluster, NGC 2682, at $\sim$ 4 Gyr (Jones, Fischer, & Soderblom 1999), we have consistently seen that a spread in lithium abundances at any one mass exists (for $M < 0.9 M_{\odot}$) up to the age of the Hyades. We also find that the stars with the highest rotation rates are all lithium-rich.

It has been speculated that rotation plays a key role in halting lithium depletion at least up until the age of NGC 1039 (250 Myr). Between this and the Hyades age, the ultra-fast rotating stars (loosely defined as those with $v \sin i > 30$ km/s) will have spun-down into the classical main-sequence distribution (Kraft 1967), and the corresponding surface lithium abundances will have settled down into a relatively

well-behaved distribution with little scatter at any given mass. Unfortunately, though, current theoretical models have not successfully explained the, perhaps fortuitous, connection between rotation and lithium depletion. In fact, rotation actually seems to produce additional mixing thereby slightly enhancing the depletion rate. This problem has been well-summarized in the work of Mendes, D'Antona & Mazzitelli (1999). Ventura et al. (1998) suggest that the missing link is the stellar magnetic field, previously disregarded in theoretical models. A strong, rotationally induced, dynamo field could inhibit convective mixing.

Extending the observational studies to younger populations of stars – the T Tauri stars (TTS) – we look for additional clues. We find that the angular momentum distribution of these stars shows a systematic difference between the mean rotation rate of the weak-lined T Tauri stars (those lacking accretion from a circumstellar disk) and that of the classical T Tauri stars which are actively accreting disk material (Rydgren & Vrba 1983, Bouvier et al. 1993, Bouvier et al. 1995, Choi & Herbst 1996). The weak-lined TTS (WTTS), on average, have shorter rotational periods than the classical TTS. Edwards et al. (1993) hypothesize that disk accretion plays an integral role in regulating the angular momentum of the classical TTS as they contract towards the main sequence. The authors suggest that those TTS whose accretion is halted early on the Hayashi track would lack this effective brake and arrive at the zero-age main sequence as rapid rotators. Since all rapid rotators (with $M < 0.9M_{\odot}$) at the ZAMS are lithium-rich compared to average depletion curves and since lithium depletion occurs on the pre-main sequence (in the range $0.2 - 0.9M_{\odot}$; Martín et al. 1994), we look for any systematic differences in the lithium abundance patterns of WTTS versus CTTS.

Two studies comparing the distribution of lithium abundances of classical and weak-lined T Tauri stars have been presented. Basri, Martín, & Bertout (1991), in a study of 28 TTS in the Taurus-Auriga star-forming complex, find no difference in the distribution of lithium abundances among classical and weak-lined TTS. Magazzù, Rebolo, & Pavlenko (1992) report similar results in their study of 36 TTS in the Ophiucus, Taurus-Auriga, NGC 2264, Chamaleon, and Lupus star-forming regions. Interestingly, Basri et al. comments that the most extreme classical TTS in their sample appear to be the most lithium-rich objects. And looking more closely at the Magazzù et al. sample, the classical TTS appear to be slightly more li-enhanced (on average) than the weak-lined TTS. While the authors do not give significance to these results, they do point out that the classical TTS, Sz 24, is extremely lithium-rich with an abundance far in excess of even the meteoritic value of the Solar system. They speculate that there might be an additional process at work providing a fresh source of lithium. Therefore, if there is any systematic difference between

the classical and weak-lined T Tauri stars, it is not evident from these studies, and, indeed, the opposite appears to be more likely.

The objective of this study is to look more carefully at the effects of the accretion process on measured lithium abundances. Studies of lithium abundances among classical TTS are fraught with pitfalls. In particular, the continuum veiling, produced by the accretion process, dilutes the stellar spectrum, making it difficult to reconstruct the true photospheric absorption. We attempt, in this study, to accurately measure the veiling in one classical TTS: RW Aur (K4; $\sim 1M_{\odot}$). This star was chosen since it is known to undergo extreme variations in its accretion as measured by the veiling. We would expect that, if accurate veiling measurement are made and the appropriate corrections are made to the observed spectrum, then reliable lithium abundances could be derived. Fourteen echelle observations of RW Aur were collected at various epochs between 1986 and 1996. Each observation presents a different veiling level. Though the accretion rate may be variable, we would expect to be able to recover a consistent surface lithium abundance. We do not. The apparent abundances change in an unexpected manner which we report herein. We discuss the implications this has on lithium depletion and accretion models.

## 2. Observations

High resolution echelle observations of RW Aur were obtained on 29 November through 1 December 1996 using the Hamilton spectrograph (Vogt 1987) fed by the 3-meter Shane telescope of Lick Observatory. Eighty-eight echelle orders spanning a wavelength range from 3820 Å to 9275 Å were recorded on a 2048 × 2048 thick Phosphor-coated CCD. The observations were made using a 640 $\mu$m slit width ($1\farcs2$ projected onto the sky) yielding $\sim 2$ pixel sampling (a resolving power of 56,000). An observing log is given in Table 1 which includes the time at mid-exposure (expressed as a heliocentric Julian date), the length of the exposure (in seconds), and the signal-to-noise per pixel at the blaze peak. These observations are supplemented by previously published data of RW Aur which are also listed in Table 1 and discussed in more detail below (§2.2).

### 2.1. Reduction and analysis

Data are reduced using the Image Reduction and Analysis Facility (IRAF). Thermal dark current corrections are found to be unnecessary. Pixel-to-pixel gain variations are removed using several spectra

Table 1. Observing Log of RW Aur

| HJD | $t_{exp}$ [s] | S/N | $v_{rad}$ [km $s^{-1}$] | vsin $i$ [km $s^{-1}$] | v [a] ($\lambda \sim 6000$) |
|---|---|---|---|---|---|
| 2450417.80447 | 3600 | 60 | -2 | 22.7 | $2.7 \pm 1.0$ |
| 2450417.94248 | 3600 | 50 | 0 | 20.5 | $1.9 \pm 0.9$ |
| 2450419.73527 | 4500 | 60 | 22 | 23.3 | $0.6 \pm 0.4$ |
| 2450419.84735 | 4500 | 45 | 18 | 22.7 | $1.0 \pm 0.6$ |
| 2450420.02697 | 5400 | 80 | 17 | 23.5 | $1.8 \pm 0.8$ |
| previously published data [b] | | | | | |
| 21 Oct 1986 | ··· | ··· | ··· | ··· | $0.3 \pm 0.3$ |
| 21 Dec 1986 | ··· | ··· | ··· | ··· | $4.8 \pm 1.6$ |
| 07 Nov 1987 | ··· | ··· | ··· | ··· | $0.8 \pm 0.4$ |
| 04 Feb 1988 | ··· | ··· | ··· | ··· | $2.4 \pm 0.9$ |
| 30 Nov 1988 | ··· | ··· | ··· | ··· | $2.0 \pm 0.9$ |
| 17 Jan 1989 | ··· | ··· | ··· | ··· | $6.1 \pm 1.7$ |
| 17 Jan 1989 | ··· | ··· | ··· | ··· | $5.0 \pm 1.4$ |
| 17 Jan 1989 | ··· | ··· | ··· | ··· | $4.4 \pm 1.3$ |
| 14 Oct 1989 | ··· | ··· | ··· | ··· | $4.4 \pm 1.6$ |

[a]Throughout this communication, we refer to the veiling – the ratio between the excess continuum emission and the photospheric continuum emission – using the symbol, v (lower case). This is to avoid confusion with the apparent magnitude , represented by V (upper case). We do not adopt the more commonly used symbol, r, in order to avoid confusion with the Pearson's r-coefficients listed in Table 3.

[b]From Basri & Batalha 1990, in which radial and rotational velocities are computed for a single observation and used for all spectra.

(combined and normalized) of a quartz-halogen incandescent lamp, filtered for more evenly distributed signal at all wavelengths. Pixel-to-pixel gain variations are typically less than ±3% in amplitude. Echelle orders are extracted following the optimal extraction algorithm of Horne (1986) and Marsh (1989). Wavelength calibration is performed by identifying over 3000 lines in the spectrum of a Thorium-Argon lamp taken with the same instrumental setup. A two dimensional polynomial fit gives the dispersion solution whose residuals (RMS) are less than $^1/_{10}$ of a pixel.

Spectral standards, taken from the catalog of Keenan & McNeil (1989), were also observed at this epoch to aid in the spectral classification of the program star as well as in the determination of radial velocity. Table 2 lists these standards and their relevant parameters. The featureless spectrum of a rapidly rotating B star, $\epsilon$ Per, was observed for the purpose of removing telluric lines from the spectra of the program star as deemed necessary. This is found to be particularly relevant for the potassium line (KI $\lambda$ 7698.977 Å). The spectral order containing this wavelength region is normalized, shifted to zero, and then scaled iteratively until the telluric lines are optimally removed from the spectrum of the program star upon subtraction.

Table 2. Spectral Standards

| HD | GJ | $\alpha$(2000) | $\delta$(2000) | SpTyp [a] | Catalog $v_{rad}$ [b] [km $s^{-1}$] | This work $v_{rad}$ [km $s^{-1}$] | vsin i [c] [km $s^{-1}$] |
|---|---|---|---|---|---|---|---|
| | | | November 1996 | | | | |
| 206301 | ··· | 21 41 33.19 | -14 02 36.1 | G2 IV | -1.2 [e] | -10.2 | ··· |
| 191026 | ··· | 20 06 22.59 | +35 58 43.0 | G8.5 IV | -33.4 [e] | -32.9 | ··· |
| 198809 | NN 4168 | 20 52 07.84 | +27 05 52.2 | G7 III | +1.0 | +8.1 | ··· |
| 117176 | 512.1 | 13 28 26.54 | +13 47 12.4 | G4 V | +5.3 | +5.2 | ··· |
| 101501 | 434 | 11 41 02.99 | +34 12 24.8 | G8 V | -5.9 | -5.3 | ··· |
| 188376 | ··· | 19 55 49.51 | -26 18 02.2 | G5 IV | -15.4 [e] | -14.9 | ··· |
| 10700 | 71 | 01 44 09.99 | -15 56 57.9 | G8 V | -17.0 | -16.7 | ··· |
| 3651 | 27 | 00 39 23.36 | +21 15 20.1 | K0 V | -32.9 | -31.4 | 0.0 |
| 10476 | 68 | 01 42 30.77 | +20 16 40.3 | K1 V | -33.7 | -33.3 | ··· |
| 20630 | 137 | 03 19 20.73 | +03 22 07.9 | G5 V | +18.9 | +19.2 | ··· |
| | | | October 1990/January 1991 | | | | |
| 3765 | 28 | 00 40 47.61 | +40 11 46.9 | K2 V | -64.2 | ··· | 0.0 |
| 223778 | 909A | 23 52 20.85 | +75 32 38.2 | K3 V | +1.7 | ··· | ··· |
| 88230 | 380 | 10 11 29.04 | +49 27 40.6 | K6 V | -25.4 | ··· | ··· |
| ··· | 908.1 | 23 50 26.79 | +30 21 10.9 | K4 V [d] | -3.1 | ··· | 3.6 |
| 19305 | 123 | 03 06 25.37 | +01 58 41.6 | M0 V | -30.2 | ··· | ··· |
| 36395 | 205 | 05 31 24.76 | -03 38 54.0 | M1.5 V | +8.5 | ··· | ··· |
| 95735 | 411 | 11 03 22.52 | +36 02 10.2 | M2 V | -84.3 | ··· | ··· |
| | | | Miscellaneous | | | | |
| 16160 | 105A | 02 36 04.89 | +06 53 12.7 | K3V | +26.0 | ··· | 2.0 |
| 32147 | 183 | 05 00 49.00 | -05 45 13.2 | K3V [e] | +22.2 | ··· | 0.0 |

### 2.2. Previously published data

Also included in this analysis are high resolution echelle spectra of RW Aur and various spectral standards taken between 1986 and 1991 by Gibor Basri and collaborators also with the 3-meter Shane telescope of Lick Observatory and the Hamilton spectrograph. The description of the RW Aur observations can be found in Basri & Batalha (1990) and Batalha et al. (1996). The additional spectral standards are listed in Table 2. It is worth noting a few significant differences between these data and the more recent observations taken November 1996. In 1994, the imaging optics of the Hamilton spectrograph were refurbished resulting in a narrower and more symmetric instrumental profile as well as a larger separation between echelle orders allowing for a more accurate determination of the scattered light surface. In addition, the older RW Aur observations were recorded on a Texas Instruments 800 × 800 CCD resulting in a more restricted spectral coverage as well as discontinuous wavelength coverage from one echelle order to the next.

### 2.3. Radial and Rotational Velocities

The radial velocity of RW Aur is determined for each independent observation of the 1996 epoch using a cross-correlation method similar to that outlined by Tonry & Davis (1979). The spectral standard, HD 3651 (K0, $v_{rad} = -32.9$), is used as the template. Its radial velocity is confirmed using the solar spectrum as reference. All echelle orders are used simultaneously in computing the cross-correlation function after filtering out atmospheric bands and stellar emission lines. The peaks of the cross-correlation functions define the radial velocities. Radial velocities are also computed for the spectral standards observed during the 1996 epoch to confirm the accuracy of the method. Both the catalog values and our determinations are listed in Table 2. For all but two stars, the differences are less than 1 km $s^{-1}$. Both HD 206301 and HD 191026 are classified as RS CVn stars, and are therefore expected to show radial velocity variations. And previously published radial velocity measurements of HD 198809 show a peak-to-peak variation of $\sim 10$ km $s^{-1}$.

Radial velocities of the RW Aur observations are listed in Table 1. The associated cross-correlation functions for the Nov 1996 observations are plotted in Figure 1. We find peak-to-peak variations of more than 20 km $s^{-1}$ – a result also obtained by Hartmann et al. (1986) – suggesting the possibility of a close companion. RW Aur is already known to be a multiple system with A and B separated by approximately $1\farcs4$ and B and C separated by approximately $0\farcs12$. With a flux ratio in the optical of 68:1 (Ghez, White, & Simon 1997), we do not expect to find contamination from RW Aur B in the spectrum of RW Aur A.

Table 2—Continued

| HD | GJ | $\alpha$(2000) | $\delta$(2000) | SpTyp [a] | Catalog $v_{rad}$ [b] [km $s^{-1}$] | This work $v_{rad}$ [km $s^{-1}$] | vsin i [c] [km $s^{-1}$] |
|---|---|---|---|---|---|---|---|
| 88230 | 380 | 10 11 22.14 | +49 27 15.3 | K6V | -25.4 | ··· | 1.9 |
| 131977 | 570A | 14 57 28.00 | -21 24 55.7 | K4V | +29.1 | ··· | ··· |
| 201091 | 820A | 21 06 53.94 | +38 44 57.9 | K5V | -64.8 | ··· | 1.3 |
| 201092 | 820B | 21 06 55.26 | +38 44 31.4 | K7V | -64.3 | ··· | 1.1 |
| 208527 | 841.1 | 21 56 23.98 | +21 14 23.5 | K5V [e] | +2.0 [e] | ··· | ··· |

[a]all but those marked taken from Keenan & McNeil 1989

[b]all but those marked taken from Gliese & Jahreiss 1991

[c]taken from Fischer 1998

[d]Fischer 1998

[d]from SIMBAD database

Ghez, White, & Simon (1997) have not found evidence of a closer companion brighter than K=10.6 down to 0.″1. However, assuming a distance of 140 pc to RW Aur, a resolution of 0.″1 corresponds to a separation of more than 6 AU. Since we see variations of more than 20 km/s over a period of just two days, we expect a closer companion to be the cause. Since there is no evidence of a secondary set of lines, we proceed with the assumption that the observed spectra are not contaminated by such a companion.

The projected rotational velocities are determined for the 1996 observations after spectral type determination (see §3). The spectrum of GJ 380 is used as the template. The entire spectrum is artificially broadened in steps of 5 km $s^{-1}$ and cross-correlated with the original spectrum. The FWHM of the resulting cross-correlation functions are then measured as a function of rotational velocity. RW Aur spectra are then cross-correlated with the template and the FWHM measured. This FWHM is then interpolated along the previously defined distribution thereby defining the projected rotational velocity. The entire echelle spectrum is strung together to make one vector which is used to compute the cross-correlation function. This results in a very high quality function with little noise. However, in practice, it is quite difficult to properly filter out all of the stellar emission lines, especially for those observations of RW Aur at high accretion rates. Emission lines produce asymmetries in the cross-correlation functions which produce systematic errors in the $v \sin i$ determinations. It is therefore plausible that the dispersion in the measurements listed in Table 1 are due to contaminating emission lines. This is currently being investigated further.

## 3. Spectral Type Estimation

For an accurate analysis of the continuum veiling, it is necessary to deduce the spectral type of RW Aur to within 2 subclasses. Errors larger than this can lead to systematic veiling errors as low (versus high) excitation potential lines yield consistently low (or high, depending on the spectral type in question) results. They also work to increase the overall scatter in veiling values measured using large numbers of absorption lines with various dependences on temperature.

To estimate the spectral type of RW Aur, we construct a grid of spectral standards ranging from G2 to

Fig. 1.— Normalized cross-correlation functions for the five observations taken in November 1996, plotted with the following symbols: HJD 2450417.80447 - diamonds; HJD 2450417.94248 - triangles; HJD 2450419.73527 - solid line; HJD 2450419.84735 - asterisks; HJD 2450420.02697 - crosses.

M2 (refer to Table 2). We select the observation of RW Aur which shows, upon simple inspection, the least veiled spectrum (HJD=2450419.73527). Spectral orders free of telluric lines and stellar emission lines are pre-selected. A result will be obtained for each of these echelle orders which will then be averaged together with all other results for the final solution.

We expect that even this low-veiled observation of RW Aur will have some excess continuum emission contaminating the underlying spectrum. We therefore proceed as follows. For each of the pre-selected echelle orders, all spectral standards are artificially veiled until the best match (lowest $\chi^2$ statistic) to the corresponding wavelength window of RW Aur is obtained. The normalized $\chi^2$ is computed for each of these solutions and that which produces the best fit is noted. In this manner, we obtain an initial veiling estimate and a spectral type for each of the spectral orders we have selected, 59 in all. GJ 908.1 provides the best match to the spectrum of RW Aur, with a veiling estimate of $0.8 \pm 0.5$.

GJ 908.1 is classified as K8V in the catalog of Gliese & Jahreiss (1991). Unfortunately, this is the only star in our sample of standards that is not classified in the Perkins Catalog of Revised MK Types (Keenan & McNeil 1989). However, in a recent, detailed analysis of K-dwarfs in the Solar neighborhood, Fischer (1998) computes (via spectral synthesis techniques) an effective temperature for this object of 4556 K – more than 400 K larger than the color temperature listed in the Gliese & Jahreiss catalog. This temperature (corresponding to K4) is confirmed using line ratio techniques. We therefore adopt a spectral type of K4 for RW Aur, consistent with the independent determination of Basri & Batalha (1990).

## 4. Veiling Determinations

### 4.1. The Method

The method used herein for determining precise veiling values is loosely based on the method described by Basri & Batalha (1990). A catalog of more than 1000 lines was constructed, and the veiling is computed on a line-by-line basis using GJ 908.1 (§3.0) as the unveiled reference. After making minor adjustments to the continuum normalization (relative to a local continuum), the template line is convolved with a rotational kernel to match the projected rotational velocity of the program star (20 km $s^{-1}$). Gaussian fits are then made to the program and template lines in question. The template gaussian is artificially veiled until a $\chi^2$ minimum is located defining the veiling value for that line.

### 4.2. Veiling Results

Figure 2 displays the resulting veiling values as a function of the rest wavelength of the line. Also shown are linear fits to the distributions. There is a general trend for the veiling to increase slightly toward bluer wavelengths. However, a single veiling value for each observation is computed by taking an average of all points between 5500 Å and 6500 Å. These values are tabulated in Table 1 and listed in Figure 2. Also listed are the number of lines yielding measurements for each observation. Obviously, as the continuum of RW Aur becomes more heavily veiled, the number of absorption lines we can detect decreases substantially (from more than 500 down to merely 35 in this case) and the noise becomes more significant. Furthermore, the older Hamilton data do not contain as broad of spectral coverage as do the newer observations. All of these factors are reflected in the dispersion (sample standard deviation) measurements which we use to estimate the uncertainty.

Veiling determinations for the older data have been previously published (Batalha et al. 1996). Our results are consistent to within the determined uncertainties.

### 4.3. Line-to-line trends

We check for any systematic line-to-line trends that may suggest the use of an inappropriate template. A difference in magnetic activity levels, for instance, may modify the T-$\tau$ relation in the TTS relative to the inactive template resulting in generally shallower line profiles. Lines formed closer to the temperature minimum will suffer more than those formed deeper in the photosphere yielding systematic errors in veiling (Finkenzeller & Basri 1987, Basri, Wilcots, & Stout 1989). Errors in effective temperature also yield systematic errors due to the fact that different lines have different dependences on temperature (Hessman & Guenther 1997).

Assuming that we have a large sample of lines and given the fact that we are more concerned with relative as opposed to absolute veiling values, neither of these errors should compromise the science

Fig. 2.— Veiling values as a function of wavelength. Each symbol represents the veiling value determined for one particular absorption line. Polynomial fits (1st order) are made to the data and the standard deviation relative to each fit is computed and listed as the uncertainty. The veiling value listed above each plot is the mean value between 5500 Å and 6500 Å.

objectives of this project. However, this is clearly not the case as we get to very large veiling values where the number of lines employed decreases significantly. Furthermore, as we look at the more heavily veiled observations, we find we are restricted to the strongest of absorption lines which may further conspire to produce systematic errors.

Plotting all of the data for a low veiling case, we find that the veiling tends to increase towards bluer wavelengths as we would expect if the continuum source is hotter that the stellar photosphere (Figure 3 a). We also note a slight increase in the average excitation potential at redder wavelengths (Figure 3 b). This casts some doubt on the wavelength dependence of the veiling distribution since our program star is undoubtedly more magnetically active than the template star. It is therefore possible that lines of low excitation potential yield systematically higher veiling values than lines of high excitation potential thereby driving the veiling distribution down towards redder wavelengths.

To check this, we quantify the veiling distribution considering only low and then only high excitation potential lines. Polynomial fits to lines of $\chi_0 > 4.5$ (56 lines) and $\chi_0 < 0.9$ (51 lines) are computed and displayed in Figure 3 c. A statistically significant increase towards the blue is found in both cases while the magnitude of the veiling decreases slightly (by $\sim 0.22$) for the high excitation potential sample. We conclude that the increase of the veiling distribution towards the blue does reflect the temperature of the emitting source. We also suspect that the absolute veiling value is influenced by a mis-match in the magnetic activity levels of the program star and the template, though the effect is smaller than the intrinsic (rms) error in the veiling measurement (0.4). Since, in this study, we are concerned with veiling variations significantly larger than 0.4, we conclude that this effect does not compromise our results even in the extreme case that our measurements for the high veiling observations are restricted only to low excitation potential lines. This, however, does not turn out to be the case. The filled symbols in Figure 3 b mark the lines used in the highest veiling observation (17 Jan 89) of RW Aur. We find we actually use more high excitation potential lines to measure the veiling of this observation.

To quantify possible errors in effective temperature, we compute the veiling distribution for the HJD 2450419.73527 observations ($v = 0.6 \pm 0.4$) using a K2 template and then an M2 template. Redward of 5500 Å, the K2 template gives an average veiling value of $0.5 \pm 0.3$ while the M2 yields $0.3 \pm 0.4$. As expected, the measured veiling value increases slightly going from the K2 to K4 template reflecting the fact that most lines are getting deeper as the star gets cooler. As we look toward an even cooler star (M2), a significant number of lines become shallower once more and the average veiling value decreases accordingly. Again, the errors we find arising from improper spectral classification are smaller than the intrinsic scatter of the

measurements and significantly smaller than the range of variations RW Aur undergoes.

## 5. The Photospheric Lines

We select a set of photospheric absorption lines which sample a relatively wide range of excitation potentials and which are not severely blended within the rotationally broadened line width. These lines are listed in Table 3. Weak (but significant) subordinate lines which lie within the rotational Doppler width are listed in parentheses.

The line equivalent width is measured for each observation of RW Aur. In order to de-veil the spectrum and recover an estimate of the true underlying photospheric line strength, we multiply each equivalent width by a factor of (1+v), where $v$ is the veiling listed in Table 1. As shown in Basri & Batalha (1990), this is the line strength one would obtain after subtracting off the excess continuum emission distribution. We make a simplification in these calculations which is to assume one average veiling value (given in Table 1) for all lines redward of 5500 Å. Changes in veiling in this wavelength range are small. The mean values of the de-veiled equivalent widths are listed in columns 4 and 11 of Table 3 for each line. In some cases, a line is not included in the spectral format of a particular observation (true for the older observations which were taken with a significantly smaller CCD) or is contaminated by bad columns, etc. Columns 6 and 13 list the number of observations for each line which yielded a measurement. Columns 3 and 10 list the (lower) excitation potential of the transition.

Figure 4 plots all of the de-veiled EW's (not the mean values listed in Table 3) as a function of veiling. For display purposes, we shift each distribution vertically so that the linear fits to the distributions are zero at the lowest veiling value. A large majority of the lines (24 out of 29, or 83%) present a constant

Fig. 3.— **a)** Veiling measurements of HJD 2450419.73527 (v=0.6) taken from Figure 2, **b)** Excitation potential (low) of lines represented in a) as a function of wavelength. The linear fit shows the slight increase of the average EP towards redder wavelengths. Filled circles mark the lines used to quantify the high-veiling observations of 17 Jan 89, **c)** The lowest EP lines ($\chi_0 < 0.9$) from a) are plotted (open circles) together with the corresponding linear fit (dashed line). The highest EP lines ($\chi_0 > 4.5$) are also plotted (filled circles) together with their linear fit (solid line). Both distributions show an increase in veiling towards the blue. The high EP lines present slightly lower veiling values, though the difference is smaller than their intrinsic (rms) dispersion.

Table 3. Line Sample and Correlation Coefficients

| ID | $\lambda$ Å | EP eV | EW [a] Å | $r$ [b] | N [c] | $t$ [d] | ID | $\lambda$ Å | $\chi_0$ eV | EW [a] Å | $r$ [b] | N [c] | $t$ [d] |
|---|---|---|---|---|---|---|---|---|---|---|---|---|---|
| CaI | 5598.48 | 2.52 | 0.34 | -0.166 | 14 | -0.584 | FeI | 7511.02 | 4.18 | 0.24 | 0.530 | 14 | 2.163 |
| (FeI) | 5598.30 | 4.65 | | | | | FeI | 7937.13 | 4.31 | 0.22 | 0.170 | 14 | 0.596 |
| CaI | 6122.22 | 1.89 | 0.79 | 0.734 | 12 | 3.420 | KI | 7698.97 | 0.00 | 1.93 | 0.964 | 14 | 12.618 |
| CaI | 6439.08 | 2.53 | 0.47 | 0.269 | 5 | 0.483 | LiI | 6707.76 | 0.00 | 0.95 | 0.902 | 14 | 7.224 |
| CaI | 6572.78 | 0.00 | 0.07 | -0.144 | 14 | -0.504 | MgI | 5528.41 | 4.35 | 0.14 | -0.482 | 14 | -1.904 |
| (CrI) | 6572.89 | 1.00 | | | | | MnI | 5394.64 | 0.00 | 0.15 | 0.118 | 14 | 0.412 |
| CrI | 7400.23 | 2.90 | 0.22 | -0.107 | 14 | -0.372 | (FeI) | 5394.68 | 4.19 | | | | |
| FeI | 5762.99 | 4.21 | 0.22 | -0.032 | 14 | -0.111 | MnI | 6021.82 | 3.07 | 0.23 | 0.293 | 13 | 1.015 |
| FeI | 5934.66 | 3.93 | 0.14 | 0.145 | 14 | 0.509 | (FeI) | 6021.79 | 2.20 | | | | |
| FeI | 6003.01 | 3.88 | 0.21 | 0.260 | 14 | 0.933 | NaI | 5688.21 | 2.10 | 0.20 | 0.609 | 6 | 1.537 |
| (VI) | 6002.62 | 1.05 | | | | | (NaI) | 5688.19 | 2.10 | | | | |
| (TiI) | 6002.63 | 2.16 | | | | | NaI | 6154.23 | 2.10 | 0.09 | 0.319 | 13 | 1.116 |
| FeI | 6020.17 | 4.61 | 0.20 | -0.414 | 14 | -1.573 | NiI | 6643.63 | 1.68 | 0.09 | -0.212 | 14 | -0.752 |
| FeI | 6024.06 | 4.55 | 0.20 | 0.412 | 13 | 1.500 | NiI | 7122.19 | 3.54 | 0.12 | -0.452 | 14 | -1.755 |
| FeI | 6400.00 | 0.91 | 0.28 | -0.272 | 14 | -0.978 | TiI | 4997.10 | 0.00 | 0.39 | 0.693 | 14 | 3.332 |
| (FeI) | 6400.32 | 0.92 | | | | | (NiI) | 4996.84 | 3.64 | | | | |
| FeI | 6430.85 | 2.18 | 0.15 | -0.180 | 13 | -0.607 | TiI | 5953.16 | 1.89 | 0.23 | 0.496 | 14 | 1.976 |
| FeI | 6633.75 | 4.56 | 0.09 | 0.508 | 14 | 2.042 | (FeI) | 5952.72 | 3.98 | | | | |
| FeI | 7130.92 | 4.22 | 0.15 | 0.277 | 14 | 1.000 | TiI | 6261.10 | 1.43 | 0.18 | 0.726 | 12 | 3.334 |
| FeI | 7495.06 | 4.22 | 0.17 | 0.014 | 14 | 0.048 | (VI) | 6261.23 | 0.27 | | | | |
| (FeI) | 7494.72 | 1.56 | | | | | | | | | | | |

[a]Average line strength over timeseries

[b]Linear correlation coefficient, or Pearson's r-coefficient.

[c]Number of measurements

[d]Student's t-distribution

equivalent width value (within our uncertainty levels), independent of veiling, as shown in the lower panel of Figure 4. This is what we'd expect to obtain assuming we have accurately recovered the purely photospheric absorption line spectrum. What is puzzling, however, is the behavior of the five lines plotted in the upper panel of the same figure: KI $\lambda$ 7699.9 Å, LiI $\lambda$ 6707.7 Å, CaI $\lambda$ 6122 Å, TiI $\lambda$ 4997 Å, and TiI $\lambda$ 6261 Å. Each of these lines appears to be enhanced by the accretion process. Figure 5 contains plots of the weaker four correlations, amplifying the y-axes for better visualization.

Linear correlation coefficients (Pearson's r-coefficients) are computed for each set of veiling/de-veiled EW parameters. These coefficients are listed in columns 5 and 12 of Table 3. To test the significance of each correlation, we compute the Student's t-statistic (tabulated in columns 7 and 14). Only the 5 lines mentioned previously show a correlation at a confidence level better than $\alpha = 0.005$ (99.5% probability that a correlation exists) as tested by this statistic. Two FeI lines ($\lambda$6633.8 and $\lambda$7511 Å) show a correlation at the $\alpha = 0.05$ confidence level. However, due to the fact that the errors are correlated –that is, an error in veiling yields a systematic and predictable error in the deveiled equivalent width – we are required to demand higher significance levels. Monte Carlo simulations reveal the nature of the correlated errors, the results of which are shown in Figure 6. The arrows mark the one-sigma deviations due to normally distributed error estimates in both parameters. Eight thousand randomly generated test points are used to test the correlated errors. The TiI $\lambda$6261 line shows only a marginal correlation at the 1-sigma level. LiI $\lambda$6707 shows a correlation at the 2-sigma level while KI $\lambda$7699 shows a correlation at the 3-sigma level (not shown in plot). And the remaining two lines, TiI $\lambda$4997 and CaI $\lambda$6122 show correlations at the 1-sigma level.

Given the large number of lines which show no correlation, and given the statistical tests described above, we conclude that the resonance lines of KI, LiI, and TiI as well as the low excitation potential line of CaI are indeed enhanced by the accretion process. We emphasize not only the low excitation potential but also the low ionization potential of these elements (4.34 - 6.11 eV). None of the low excitation potential lines of the higher IP elements, FeI, NiI, and MnI (7.43 - 7.87 eV), show any indication of a correlation with veiling at our detection level. Using the catalogue of solar lines (Moore, Minnaert, & Houtgast 1966) and the VALD database, we search for other resonance lines which could contribute to our sample, especially those of low IP elements such as TiI, VI, RbI, and CsI. Unfortunately, we are unable to identify any additional lines whose equivalent widths can be recovered at all (or nearly all) veiling values and whose rotationally broadened line width is not overwhelmingly blended. We measure a weak resonance line of RbI ($\lambda$7800.3 Å) in the low veiling observations. Although this line is of great interest due to its low ionization

potential (4.18 eV), we are unable to detect measurable absorption in the highly veiled spectra.

## 6. Discussion

### 6.1. Line Enhancement Mechanisms

We note that the lines showing accretion-induced enhancements are resonance lines (or low excitation potential lines) of low ionization potential elements. With this in mind, we consider the possible mechanisms which may be at work.

Dark spots arising from localized concentrations of surface magnetic flux can increase the disk-integrated equivalent width of temperature sensitive lines (those who increase in strength going from photospheric to cooler spot temperatures). This is the case for the resonance lines of lithium and potassium. However, the effect is predicted to be small (e.g. $\sim 7\%$ for KI $\lambda$7699 Å in a K6 photosphere with a 14% spot filling factor, and 3000K spot temperature (Stout-Batalha 1997)) compared to the large enhancements observed herein (300% for lithium, for example). Observations also reveal that the disk-integrated effect of surface spots is small. Less than a 15% change in line strength is observed in the lithium resonance line as the large area spots of HII 686 and HII 3163, two ultra-fast rotating ZAMS stars of the Pleiades, rotate in and out of view (Stout-Batalha & Vogt 1999). Similar results are found for the rapidly rotating, weak-lined T Tauri stars, P1724 (Neuhäuser et al. 1998) and Oph 052 and Oph 120S (Patterer et al. 1993). Considering the typically slow rotation rates of classical TTS (and RW Aur as implied by its small projected rotational velocity), we find it very unlikely that the line enhancements are a consequence of dark spots.

We entertain the idea that the line enhancements are true elemental abundance variations, perhaps furnished by disk accretion. This is perhaps appealing for the lithium enhancements since the surface abundances may be slightly depleted through convective mixing for a star of this estimated mass ($\sim 1 M_{\odot}$; Bertout, Basri, & Bouvier 1988) and age (Mendes, D'Antona, & Mazzitelli 1999). However, this quickly

Fig. 4.— Deveiled equivalent widths are measured for each line and each observation of RW Aur and then plotted against the veiling. 24 out of 29 lines show no correlation between these two parameters (lower panel). However, the 5 lines plotted in the upper panel all yield a significant correlation as tested by computing linear correlation coefficients and comparing these against the Student's t-distribution, both of which are tabulated in Table 3.

proves to be unlikely. If we compute surface lithium abundances using de-veiled lines (see §6.4), we recover values (at intermediate accretion rates) more than an order of magnitude larger than the primordial (meteoritic) lithium abundance. Moreover, variations occur on timescales shorter than one day. We could not explain this considering the accretion of a relatively small amount ($10^{-7} - 10^{-8} M_{\odot} yr^{-1}$; Valenti et al. 1993, Hartigan, Edwards, & Ghandour 1995) of disk gas of no more than meteoritic number densities of lithium, onto the stellar surface. Finally, we are still left with the additional problem of explaining the even larger potassium enhancements, impossible to reconcile if we are correct in assuming that the disk and stellar abundances of potassium should be nearly identical. This should also be true for titanium.

We consider the presence of a low temperature component to the accretion flow which could furnish a significant number of neutral species of the elements in question. The gas temperature and density should yield the strongest enhancements in potassium, followed by lithium and then titanium, with no enhancements measured in the higher IP element, manganese. In the following section, we present simple slab models which suggest that the presence of such a cool gas could explain the various enhancements we observe. We then compute line bisectors which suggest that the excess absorption indeed arises in an infalling gas.

### 6.2. Slab Models

The distribution of cold gas around RW Aur is approximated by an isothermal slab model characterized by temperature, density and physical depth. Line and continuum opacities are computed over a range of temperatures (1250 to 4000 K) and densities ($\log N_H = 11.0 - 17.0$ cm$^{-3}$) while holding the physical depth (0.1 R$_*$) and surface area (100% of stellar surface) constant. The objective is to determine, qualitatively, if a cold gas can yield the relative enhancements in the resonance lines of KI, LiI, TiI, and MnI. We also include RbI $\lambda$7800.3 Å in the analysis even though we do not have a complete set of measurements (see §5) for this resonance line. It is weak ($\sim$ 100 mÅ) in the spectrum of our K4 templates but becomes pronounced in the spectra of L stars (below 2200 K). The fact that we do not detect this line in the highly veiled observations is an additional constraint on the gas temperature in the slab. Standard continuum opacity sources are included as a means of checking the global stellar extinction. We demand that the circumstellar gas remains

Fig. 5.— The upper panel of Figure 4 is reproduced here, once for each of the LiI, CaI, and TiI lines, with the y-axis amplified to better illustrate these weaker correlations.

optically thin in the continuum. Level populations which control the line opacities are computed under the assumption of LTE.

The lines of the best matching spectral standard (GJ 908.1) are used as input to represent the photospheric contribution except in the case of lithium. For the $\lambda$6707 resonance line, the low veiling observation of HJD 2450419.73527 (de-veiled) is used as input. We proceed by computing the equivalent widths of the (first) veiled and (then) extincted line profiles for the highest veiling state we observe (v=6.1) over the above-mentioned grid of slab temperatures and densities. These equivalent widths are then de-veiled in order to obtain consistency with the observed quantities plotted in Figures 4 to 6.

Figure 7 shows the results. Plotted are the computed line strengths as a function of hydrogen number density at a slab temperature of 2000K, valid for the highest veiling observation (17 Jan 89; v=6.1). Horizontal lines show the observed (de-veiled) line strengths of each element. The hatched area corresponds to the one-sigma uncertainty levels in these observed quantities. A slab temperature of 2000 K and density of $\log N_H \sim 16$ (marked by vertical line) is able to reproduce the observed line strengths. In the case of MnI, we find that the slab provides no additional line extinction, consistent with our observations. In the case of RbI, the slab does furnish a small degree of extinction. However, at this temperature and at $\log N_H = 16$, the resulting line strength is less then 200 mÅ. Lines weaker than this will not be observable at our signal-to-noise in such a highly veiled spectrum.

We do not suggest that our computed slab parameters are necessarily physically meaningful. The accretion flow is not well represented by an isothermal slab of uniform density as has been shown by magnetic accretion models (Martin 1996, Muzerolle, Calvet, & Hartmann 1998, Calvet & Gullbring 1998). However, assuming the line enhancements are produced in approximately the same region, such a simplified representation is useful and suggests that a cold component of the accretion flow can yield the relative line enhancements observed.

Observational constraints to magnetospheric accretion models are commonly provided by the emission line spectrum as well as the excess continuum emission. Both diagnostics probe hot regions. Muzerolle, Calvet, & Hartmann (1998) find that average temperatures of the accretion flow must reach 6000 - 10000 K in order to reproduce the hydrogen emission lines. Martin (1996) computes self-consistent models of

Fig. 6.— Monte Carlo simulations are run to test the effect of correlated errors in veiling (x-axis) and the de-veiled EW's (y-axis). Arrows mark the $\pm 1\sigma$ deviations.

the thermal structure of gas inflowing along magnetic field lines for a star with typical CTTS properties. Temperatures reach peak values of 6500 - 8000 K, depending on the accretion rate. However, the initial gas temperature in the region where the magnetic field disrupts the disk ($3.4 - 5R_*$, in his models) is arbitrarily fixed at 3000 K. To date, we lack an onservational parameter to constrain this quantity. Since we do not observe large velocities of the excess absorption, this is precisely the region of interest – the region we believe the line enhancements are probing. This is discussed further in §6.3.

Investigating the effect of various accretion rates on the thermal structure, Martin finds that inefficient heating and efficient cooling at high accretion rates result in lower average temperatures in the accretion flow. In particular, he considers accretion rates of $10^{-6}$, similar to that estimated for RW Aur (Hartigan, Edwards, & Ghandour 1995). The thermal structure, though tied to 3000 K at the disk midplane, decreases to 2000 K before rising again as it approaches the stellar surface. Such low temperatures are favorable for explaining the line enhancements reported herein.

### 6.3. Line Bisectors

We search for any telltale asymmetries in the line profiles which may indicate bulk motion in the gas giving rise to the excess absorption. For this purpose, we compute the line bisectors of the LiI and KI resonance lines obtained in November 1996 (see Table 1). We concentrate on this subsample of observations due to the higher precision of the wavelength calibration and radial velocity determinations.

Displayed in the upper panel of Figure 8 are the line bisectors of the LiI and KI resonance lines for two low veiling observations (HJD 2450419.73527, HJD 2450419.84735 – diamonds) and two high veiling observations (HJD 2450417.80447, HJD 2450417.94248 – asterisks). The lowest veiling observation of RW Aur during the 1996 season is overplotted for reference. A completely symmetric line profile would produce a perfectly vertical line bisector. Blends produce systematic deviations in the line bisectors of all observations, independent of veiling . But the high veiling observations show additional deviations towards

Fig. 7.— Modeled line equivalent widths are plotted as a function of hydrogen number density (log scale) for a slab model of uniform temperature (2000 K), of thickness $0.1R_*$, covering 100% of the stellar surface. Horizontal lines mark the observed equivalent widths in RW's highest veiling state (17 Jan 89). At a density of $N_H \sim 10^{16}$, we recover consistent line strengths in all resonance lines (to within the measured uncertainty levels shown as the hatched area). MnI shows no significant enhancement, consistent with observations.

the red. This can be seen qualitatively in the middle panels which contain the (de-veiled) profiles of the lowest (solid line; HJD 2450419.73527; v=0.6) and the highest (dashed line; HJD 2450417.80447; v=2.7) veiling observations of November 1996. It is evident that much of the excess absorption generated by the accretion process is redshifted relative to line center. Subtraction of the two veiling states yields redshifted residual absorption profiles (lower panel) with line centroids at 9.8 km $s^{-1}$ for LiI and 19.5 km $s^{-1}$ for KI. This lends further support to the hypothesis that the line enhancements arise in an infalling gas and probe relatively low-velocity, low-temperature regions near the co-rotation radius.

### 6.4. Systematic Errors in Lithium Abundance Determinations

Using two high-quality, high-spectral coverage observations of RW Aur (HJD 2450417.80447,v=2.7; HJD 2450419.73527,v=0.6), we de-veil the spectral regions containing the lithium resonance lines at 6707.7 Å and use the resulting profiles to compute the LTE lithium abundances. We employ the spectral synthesis code, SME, described in Valenti & Piskunov (1996) and the line lists returned by the VALD database (Piskunov et al. 1995). The code includes a Marquardt non-linear least squares algorithm which allows the user to simultaneously solve for selected stellar and/or atomic parameters which minimize the $\chi^2$ statistic. In this manner, we obtain a lithium abundance of $\epsilon(N_{Li}) = 3.2$ for the low veiling observation and $\epsilon(N_{Li}) = 4.4$ for the more highly veiled observation. The lower veiling observation gives us a better estimate of the true lithium abundance on the stellar surface in light of the results presented in §5. We find a slightly depleted lithium abundance relative to meteoritic values qualitatively in keeping with theoretical predictions. However, at a veiling of 0.6, this is still likely to be an over-estimate. As expected, the

Fig. 8.— Line bisectors (upper panel) of the LiI and KI resonance lines are computed for two low veiling (HJD 2450419.73527, HJD 2450419.84735) and two high veiling (HJD 2450417.80447, HJD 2450417.94248) observations of RW Aur. Diamonds mark the line bisectors of the low veiling observations while asterisks mark those of the high veiling observations. Deviations toward the red are clearly seen in the case of high veiling. This can be seen qualitatively in the middle panel in which the lowest veiling (solid line; HJD 2450419.73527; v=0.6) and the highest veiling (dashed line; HJD 2450417.80447; v=2.7) observation of each line is plotted (after de-veiling). Subtraction yields residual absorption (lower panel; asterisks). Line centroids (vertical line) of the residual absorption are computed via gaussian fits (solid line) and listed in the bottom right corner.

high veiling observation of RW Aur yields an abundance significantly larger than meteoritic values as has previously been found for a handful of other CTTS (Basri, Martín, & Bertout 1991, Magazzù, Rebolo, & Pavlenko 1992). We conclude that the accretion-enhanced line strengths of lithium can lead to gross over-estimates in the true surface abundance.

## 7. Conclusions

We present, in this communication, a study of high resolution echelle spectra of the classical T Tauri star, RW Aur, taken sporadically over a period of more than 10 years. The continuum veiling distribution is determined in the optical by comparing hundreds of stellar absorption lines of a well-matching spectral template star with those of the program star. Errors (both random and systematic) in the resulting veiling values are investigated. We find that systematic errors arising from improper spectral classification are less than the actual line-to-line dispersion in the veiling values and significantly smaller than the magnitude of the veiling variations which RW Aur undergoes.

In the process of investigating LiI $\lambda$6707.7 Å as a potential veiling diagnostic (useful in cases of extremely high continuum veiling which works to wash away all but the strongest absorption lines), we find that this particular absorption line is, in fact, enhanced by the accretion process. Its line strength (after applying corrections for the effect of continuum veiling) more than doubles between the observation of lowest measured accretion and that of the highest measured accretion. Searching for similar behavior among other resonance lines of low IP elements, we find that KI ($\lambda$7699.9 Å) and TiI ($\lambda$4997.1 Å) are also enhanced by the accretion process, thereby eliminating the possibility that lithium undergoes true abundance variations as the disk supplies fresh lithium which convective mixing then works to deplete. We conclude that the observed line enhancements are significant, and not merely a consequence of errors in veiling determinations, after finding no such enhancements in a large sample of absorption lines of different excitational potentials and of various IP elements. Approximately 83% of the 29 lines studied show no correlation at all between their line strength and the respective continuum veiling.

We find that the resonance line of the lowest IP element observed, KI (4.34 eV), presents the most sensitive correlation between veiling and line strength, followed by that of LiI (5.39 eV) and then TiI (6.82 eV). The resonance line of MnI (7.43 eV) shows no similar behavior. Finding it unlikely that cool magnetic surface spots are responsible for the observed enhancements, we investigate the possibility of an additional source of line opacity arising in a cool gas in the accretion flow. Simple slab models are generated which

successfully reproduce the relative line enhancements observed among the 4 resonance lines of KI, LiI, TiI, and MnI at a temperature of 2000 K and density of $\log N_H \sim 16$. Models assume a projected thickness of $0.1R_*$ and a filling factor of 100% (that is, the entire stellar surface is assumed to be extincted by the accreting gas). While providing line extinction, the slab does not introduce significant continuum opacity.

Line bisectors of the KI line profiles are computed, and comparison of those of the low veiling observations with those of the high veiling observations reveal that the excess absorption is preferentially redshifted relative to the stellar rest-frame. The bisectors of the low and high veiling states differ by merely 10 km s$^{-1}$ for LiI and 20 km s$^{-1}$ for KI. Centroids of the residual absorption yield the same results. This leads us to speculate that the line enhancements are indeed generated in an infalling gas located at the beginning of the accretion flow near the co-rotation radius.

As an exercise, the surface lithium abundances are computed using veiling-corrected $\lambda$6707.7 Å line profiles and ignoring the accretion-induced enhancements. We find that, as a consequence, surface lithium abundances can be grossly over-estimated. At a veiling of 0.6, we compute an LTE abundance of $\epsilon(N_{Li}) = 3.2$, while at a veiling of 2.7, we compute an abundance of $\epsilon(N_{Li}) = 4.4$. We hypothesize that the large abundances (often in excess of meteoritic values) reported for the highly accreting TTS suffer from such systematic errors.

We conclude that the resonance lines of LiI, KI, and TiI are unreliable lines for measuring continuum veiling in classical TTS. However, they may act as an additional probe of the circumstellar environment which has traditionally been left to the emission line spectrum. We propose that a cool component to the accretion column could explain the observed line enhancements of the low IP resonance lines studied herein. We also conclude that surface lithium abundance measurements of classical TTS are subject to gross systematic errors. Such errors can be minimized by studying systems, such as RW Aur, which present largely varying accretion rates. In its low accretion state, RW Aur presents a slightly depleted surface lithium abundance, as is predicted by theoretical models for a star of this age and mass.

This work was supported by the Fundação de Amparo à Pesquisa do Estado do Rio de Janeiro (FAPERJ). We thank E. Martín for his careful reading of this manuscript.

## REFERENCES

Anders, E., Grevesse, N. 1989, Geochim. Cosmochim. Acta, 53, 197

Balachandran, S., Lambert, D.L., Stauffer, J.R. 1988, Astrophys. J., 333, 267

Basri, G.S., Batalha, C.C. 1990, Astrophys. J., 363, 654

Basri, G., Marcy, G.W., Graham, J.R. 1996, Astrophys. J., 458, 600

Basri, G., Martín, E.L. 1999, Astrophys. J., 510, 266

Basri, G., Martín, E.L., Bertout, C. 1991, Astron. Astrophys., 252, 625

Basri, G., Wilcots, E., Stout, N. 1989, Publ. Astron. Soc. Pac., 101, 528

Batalha, C.C., Stout-Batalha, N.M., Basri, G.S., Terra, M.A.O. 1996, Astrophys. J., Suppl. Ser., 103, 211

Bertout, C., Basri, G., Bouvier, J. 1988, Astrophys. J., 330, 350

Bodenheimer, P. 1965, Astrophys. J., 142, 451

Bonsack, W.K., Greenstein, J.L. 1960, Astrophys. J., 131, 83

Bouvier, J., Cabrit, S., Fernández, M., Martín, E.L. and Matthews, J.M. 1993, Astron. Astrophys., 272, 176

Bouvier, J., Covino, E., Kovo, O., Martín, E.L., Matthews, J.M., Terranegra, L. and Beck, S.C. 1995, Astron. Astrophys., 299, 89

Calvet, N. and Gullbring, E. 1998, Astrophys. J.. 509, 802

Cayrel, R., Cayrel de Strobel, G., Campbell, B., Däppen, W. 1984, Astrophys. J., 283, 205

Choi, P.I. and Herbst, W. 1996, Astron. J., 111, 283

Edwards, S., Strom, S.E., Hartigan, P., Strom, K.M., Hilenbrand, L.A., Herbst, W., Attridge, J., Merril, K.M., Probst, R., Gatley, I. 1993, Astron. J., 106, 372

Finkenzeller, U., Basri, G. 1987, Astrophys. J., 318, 823

Fischer, D.A. 1998, Ph.D. thesis, University of California, Santa Cruz

García-Lopez, R.J., Rebolo, R., Martín, E.L. 1994, Astron. Astrophys., 282, 518

Ghez, A.M., White, R.J., Simon, M. 1997, Astrophys. J., 490, 353

Gliese, W., Jahreiss, H. 1991, *Catalog of Nearby Stars*, Veroff. Astron. Rechen-Inst., Heidelberg, third edition

Gullbring, E., Hartmann, L., Briceno, C., Calvet, N. 1998, Astrophys. J., 492, 323

Hartigan, P., Edwards, S., Ghandour, L. 1995, Astrophys. J., 452, 736

Hartmann, L., Hewett, R., Stahler, S., Mathieu, R. 1986, Astrophys. J., 309, 275

Hessman, F.V., Guenther, E.W. 1997, Astron. Astrophys., 321, 497

Horne, K. 1986, Publ. Astron. Soc. Pac., 98, 609

James, D.J., Jeffries, R.D. 1997, Mon. Not. R. Astron. Soc., 292, 252

Jeffries, R.D., James, D.J., Thurston, M.R. 1998, Mon. Not. R. Astron. Soc., 300, 550

Jones, B.F., Fischer, D., Shetrone, M., Soderblom, D.R. 1997, Astron. J., 114, 352

Jones, B.F., Fischer, D., Soderblom, D.R. 1999, Astron. J., 117, 330

Jones, B.F., Shetrone, M., Fischer, D., Soderblom, D.R. 1996, Astron. J., 112, 186

Keenan, P.C., McNeil, R.C. 1989, Astrophys. J., Suppl. Ser., 71, 245

Kraft, R.P. 1967, Astrophy. J., 150, 551

Magazzù, A., Rebolo, R., Pavlenko, Ya.V. 1992, Astrophys. J., 392, 159

Marsh, T. 1989, Publ. Astron. Soc. Pac., 100, 1032

Martín, E.L., Montes, D. 1997, Astron. Astrophys., 318, 805

Martín, E.L., Rebolo, R., Magazzù, A., Pavlenko, Ya.V. 1994, Astron. Astrophys., 282, 503

Martin, S.C. 1996, Astrophys. J., 470, 537

Mendes, L.T.S., D'Antona, F., Mazzitelli, I. 1999, Astron. Astrophys., 341, 174

Moore, C.E., Minnaert, M.G.J., Houtgast, J. 1966, The Solar Spectrum 2935 Å to 8770 Å, National Bureau of Standards Monograph 61

Muzerolle, J., Calvet, N., Hartmann, L. 1998, Astrophys. J., 492, 743

Neuhäuser, R., Wolk, S.J., Torres, G., Preibisch, Th., Stout-Batalha, N.M., Hatzes, A.P., Frink, S., Covino, E., Walter, F.M., Alcala, J.M., Sterzik, M.F. and Wichmann, R. 1998, Astron. Astrophys., 334, 873

Nichiporuk, W., Moore, C.B. 1974, Geochim. Cosmochim. Acta, 38, 1691

Patterer, R.J., Ramsey, L., Huenemoerder, D.P., Welty, A.D. 1993, Astron. J., 105, 1519

Piskunov, N.E., Kupka, F., Ryabchikova, T.A., Weiss, W.W. and Jeffery, C.S. 1995, Astron. Astrophys., Suppl. Ser., 112, 525

Randich, S., Aharpour, N., Pallavicini, R., Prosser, C.E., Stauffer, J.R., Schmitt, J.H.M.M. 1996, Proceedings of the 9th Cambridge Workshop on Cool Stars, Stellar Systems, and the Sun, Astronomical Society of the Pacific Conference Series, volume 109, edited by Roberto Pallavicini and Andrea K. Dupree, p.379

Randich, S., Martín, E.L., García López, R.J., Pallavicini, R. 1998, Astron. Astrophys., 333, 591

Rydgren, A.E. and Vrba, F.J. 1983, Astrophys. J., 267, 191

Soderblom, D.R., Fedele, S.B., Jones, B.F., Stauffer, J.R., Prosser, C.F. 1993a, Astron. J., 106, 1080

Soderblom, D.R., Jones, B.F., Balachandran, S., Stauffer, J.R., Duncan, D.K., Fedele, S.B., Hudon, J.D. 1993b, Astron. J., 106, 1059

Soderblom, D.R., Jones, B.F., Stauffer, J.R., Chaboyer, B. 1995, Astron. J., 110, 729

Stauffer, J.R., Schultz. G., Kirkpatrick, J.D. 1998, Astrophys. J., Lett., 499, 199

Stout-Batalha, N.M., Ph.D. thesis, University of California, Santa Cruz

Stout-Batalha, N.M., Vogt, S.S. 1999, Astrophys. J., Suppl. Ser., 123, ???

Thorburn, J.A., Hobbs, L.M., Deliyannis, C.P., Constantine, P., Pinsonneault, M.H. 1993, Atrophys. J., 415, 150

Tonry, J. and Davis, M. 1979, Astron. J., 84, 1511

Valenti, J.A., Basri, G., Johns, C.M. 1993, Astron. J., 106, 2024

Valenti, J.A. and Piskunov, N. 1996 Astron. Astrophys., Suppl. Ser., 118, 595

Ventura, P., Zeppieri, A., Mazzitelli, I., D'Antona, F. 1998, Astron. Astrophys., 331, 1011

Vogt, S.S. 1987, Publ. Astron. Soc. Pac., 99, 1214

Zappala, R.R. 1972, Astrophys. J., 172, 57

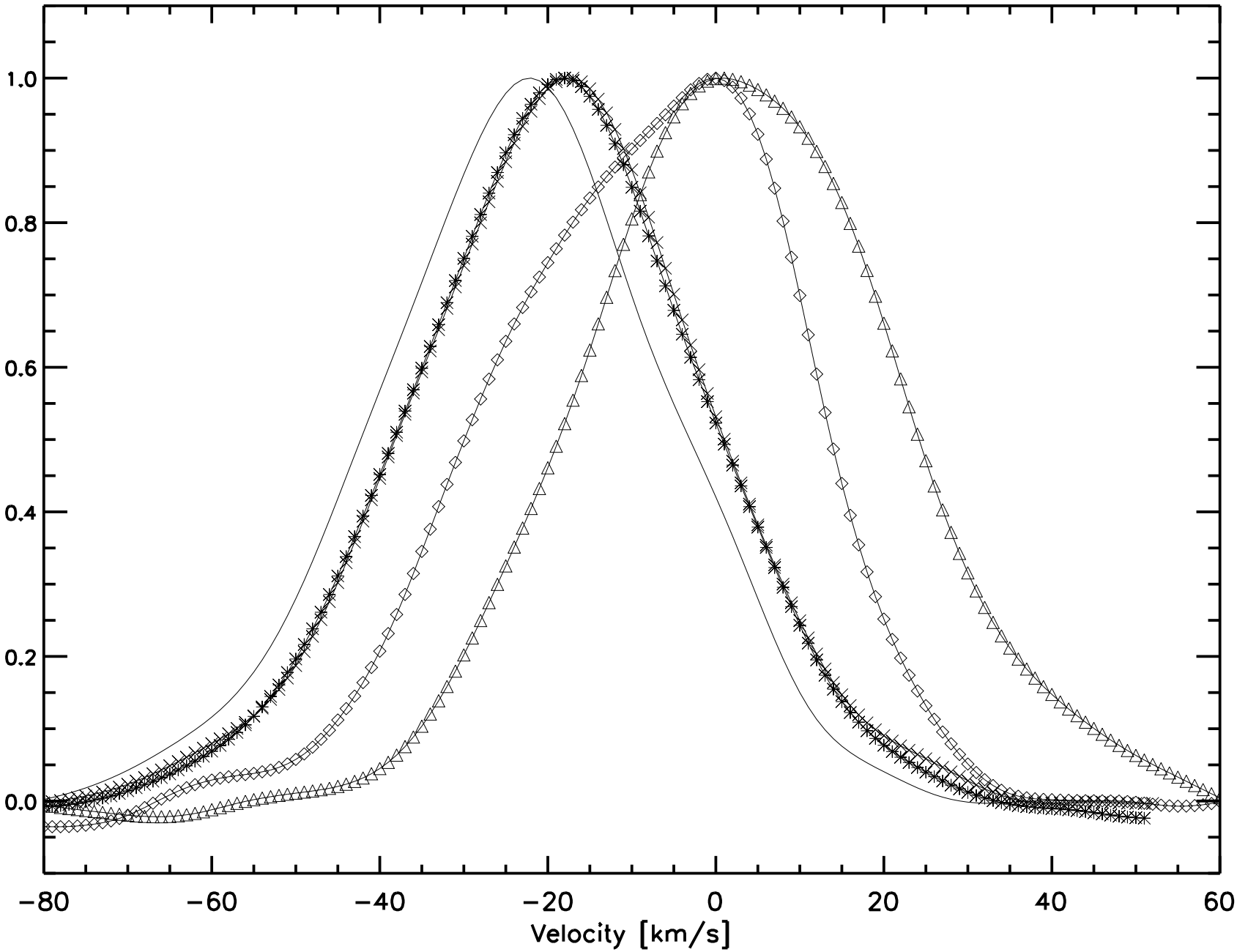
1.0
0.8
0.6
0.4
0.2
0.0
−80
−60
−40
−20
0
20
40
60
Velocity [km/s]

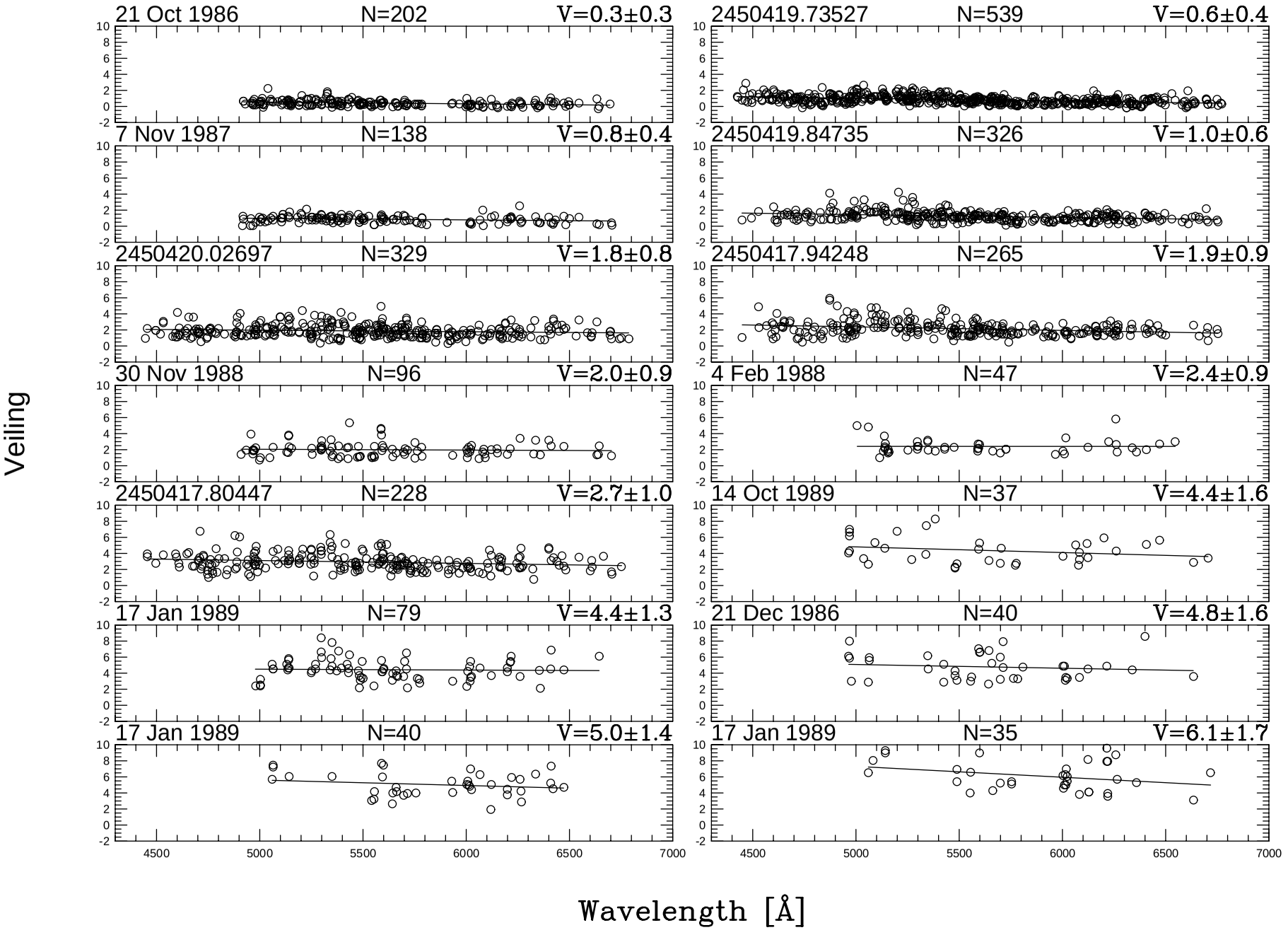
21 Oct 1986 N=202 V=0.3±0.3
2450419.73527 N=539 V=0.6±0.4
7 Nov 1987 N=138 V=0.8±0.4
2450419.84735 N=326 V=1.0±0.6
2450420.02697 N=329 V=1.8±0.8
2450417.94248 N=265 V=1.9±0.9
30 Nov 1988 N=96 V=2.0±0.9
4 Feb 1988 N=47 V=2.4±0.9
2450417.80447 N=228 V=2.7±1.0
14 Oct 1989 N=37 V=4.4±1.6
17 Jan 1989 N=79 V=4.4±1.3
21 Dec 1986 N=40 V=4.8±1.6
17 Jan 1989 N=40 V=5.0±1.4
17 Jan 1989 N=35 V=6.1±1.7
Veiling
Wavelength [Å]

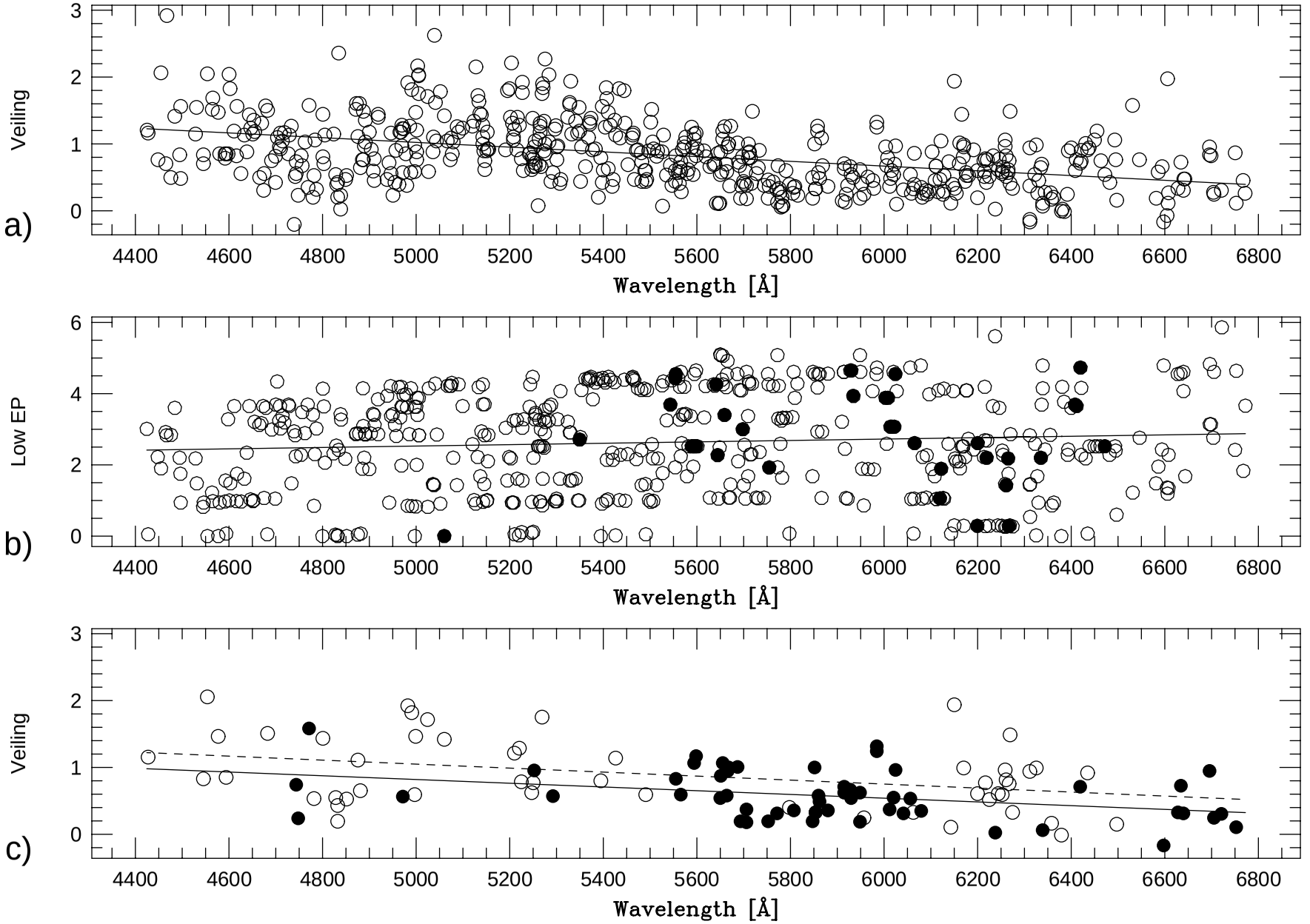
a)
Veiling
3
2
1
0
4400
4600
4800
5000
5200
5400
5600
5800
6000
6200
6400
6600
6800
Wavelength [Å]
b)
Low EP
6
4
2
0
4400
4600
4800
5000
5200
5400
5600
5800
6000
6200
6400
6600
6800
Wavelength [Å]
c)
Veiling
3
2
1
0
4400
4600
4800
5000
5200
5400
5600
5800
6000
6200
6400
6600
6800
Wavelength [Å]

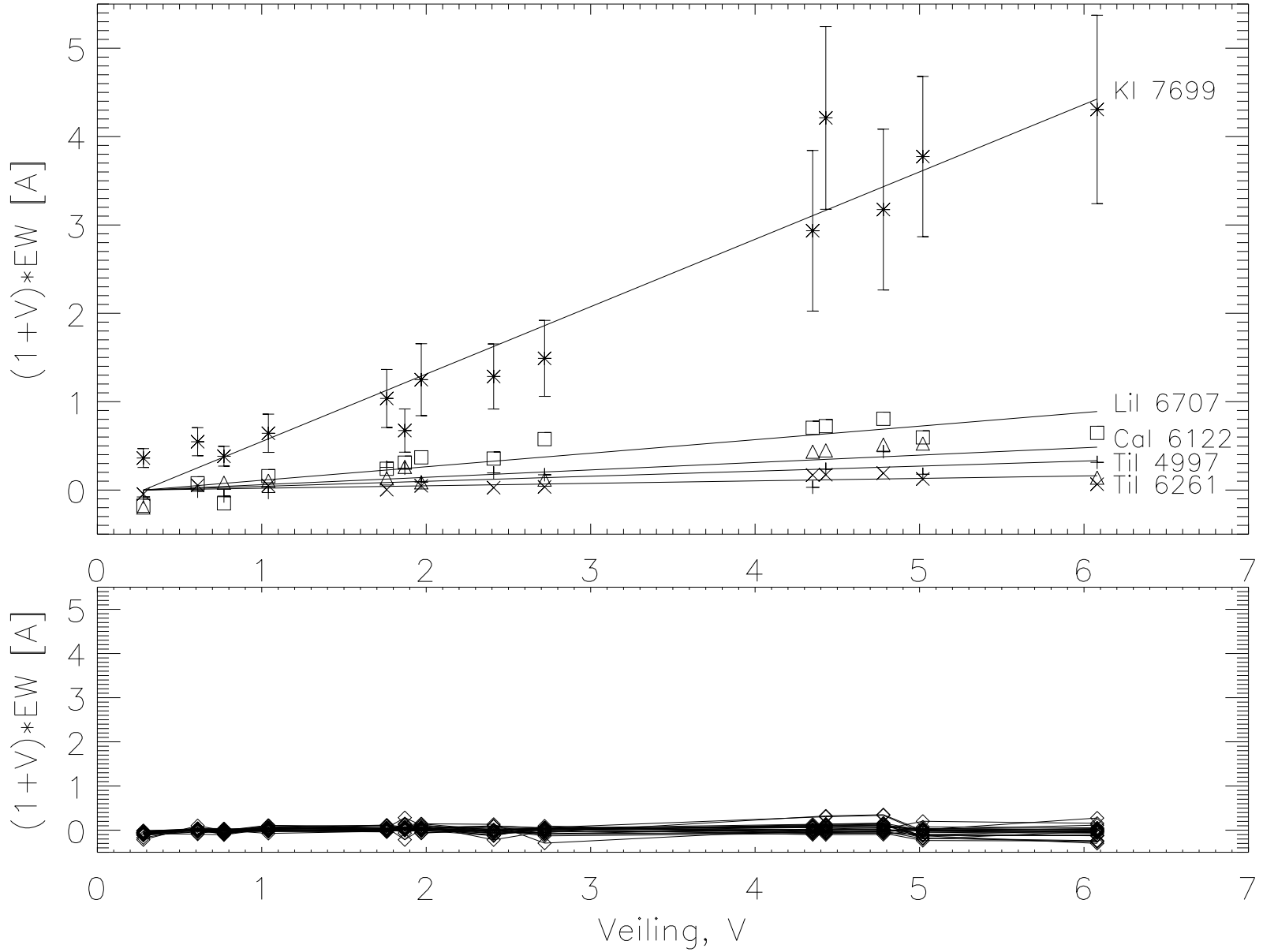
(1+V)*EW [A]
KI 7699
LiI 6707
CaI 6122
TiI 4997
TiI 6261
(1+V)*EW [A]
Veiling, V

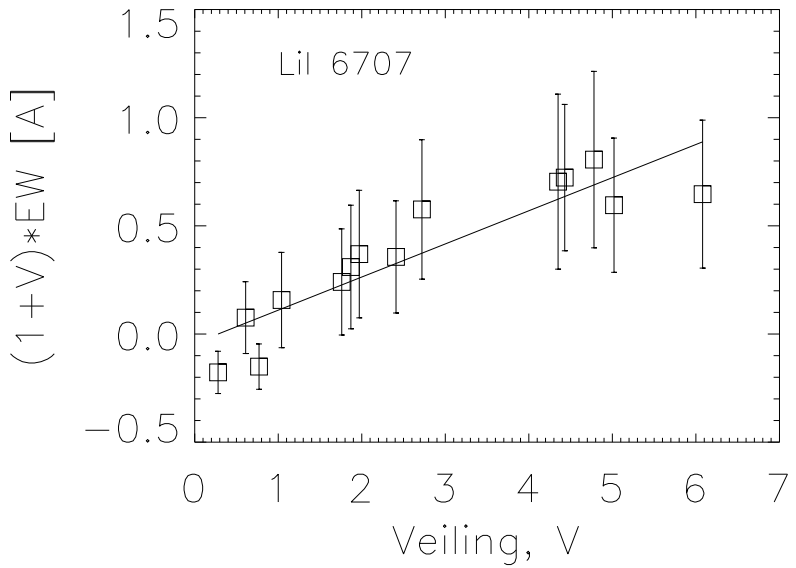
LiI 6707
(1+V)*EW [A]
Veiling, V
1.5
1.0
0.5
0.0
−0.5
0
1
2
3
4
5
6
7

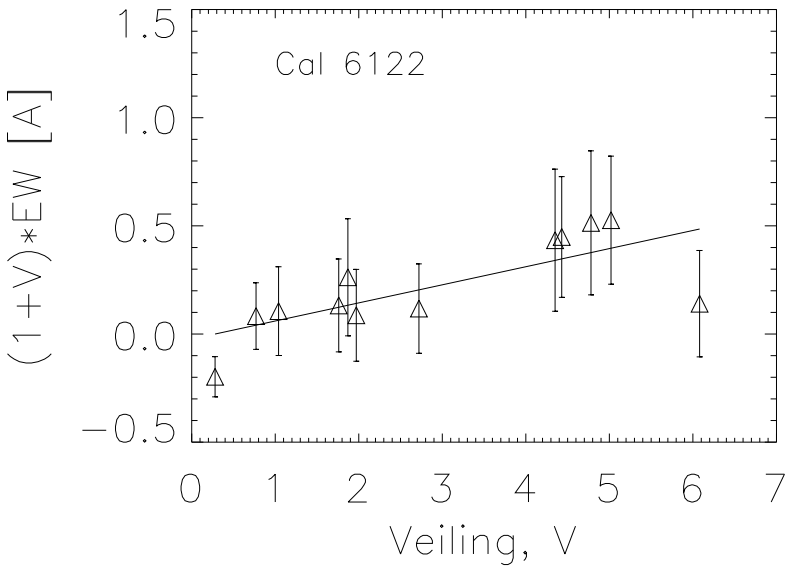
CaI 6122
(1+V)*EW [A]
Veiling, V
1.5
1.0
0.5
0.0
−0.5
0
1
2
3
4
5
6
7

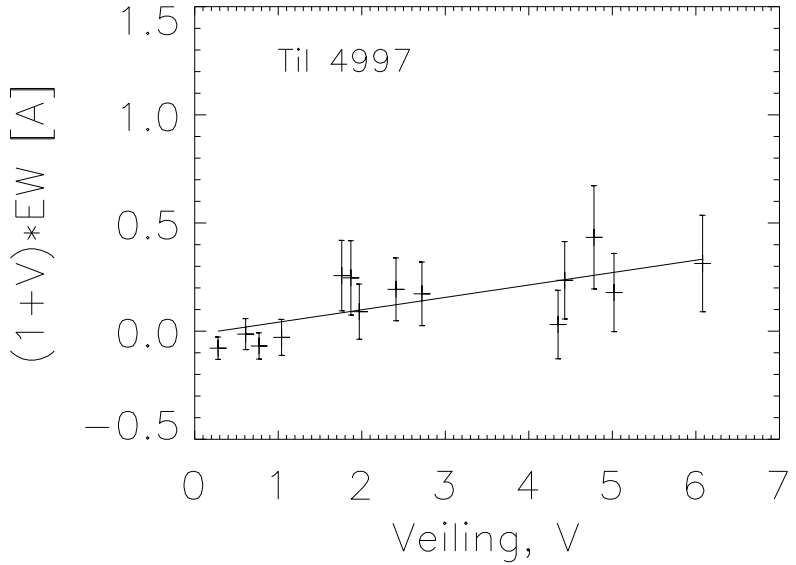
TiI 4997
(1+V)*EW [A]
Veiling, V
1.5
1.0
0.5
0.0
−0.5
0
1
2
3
4
5
6
7

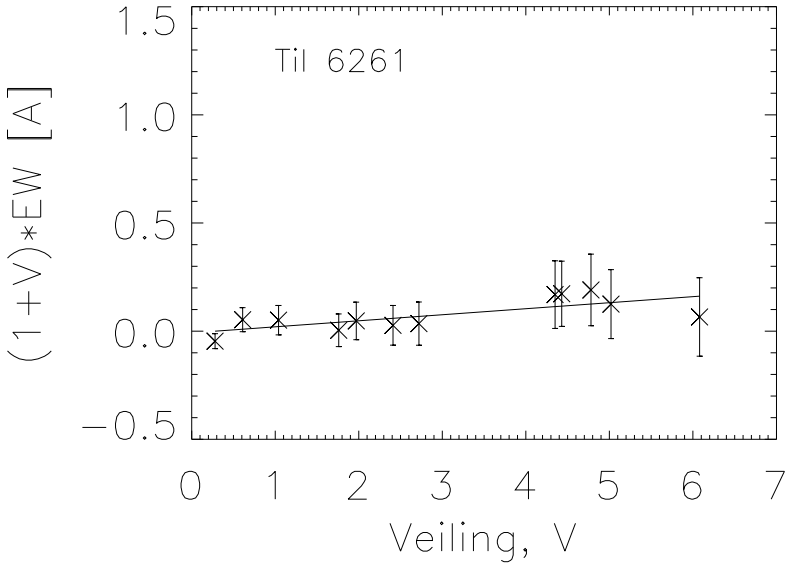
TiI 6261
(1+V)*EW [A]
Veiling, V
1.5
1.0
0.5
0.0
−0.5
0
1
2
3
4
5
6
7

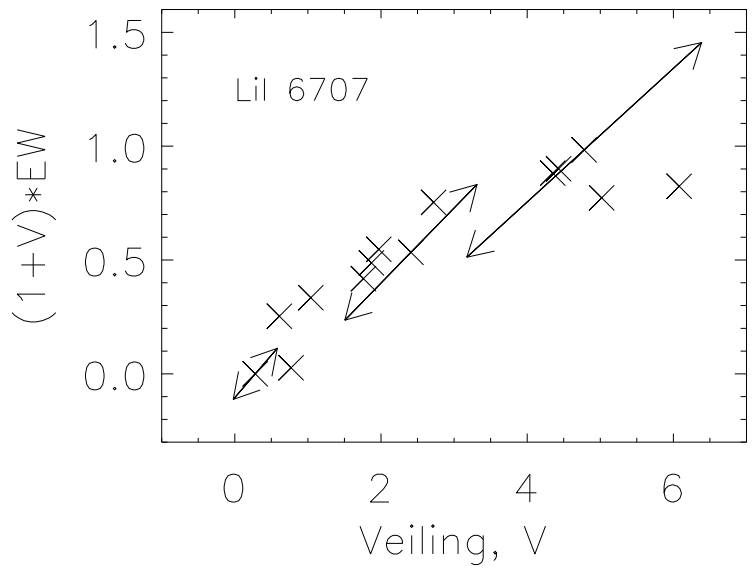
LiI 6707
(1+V)*EW
Veiling, V
0.0
0.5
1.0
1.5
0
2
4
6

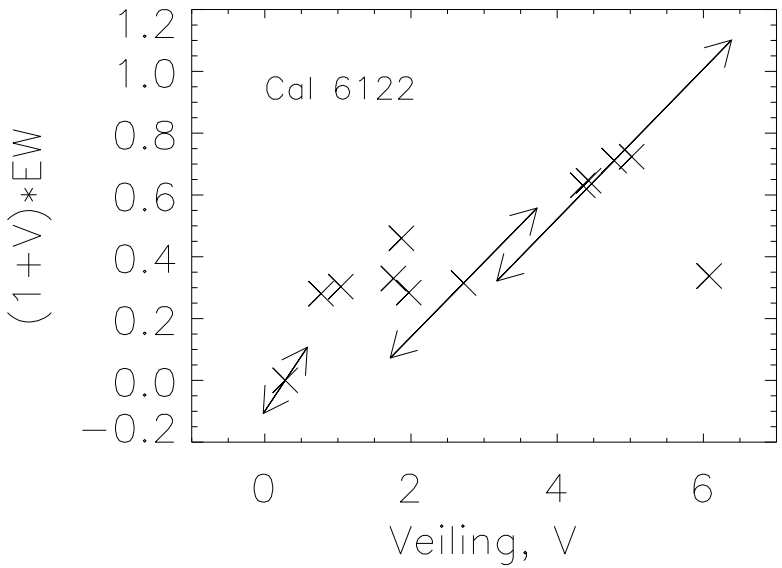
CaI 6122
(1+V)*EW
Veiling, V
−0.2
0.0
0.2
0.4
0.6
0.8
1.0
1.2
0
2
4
6

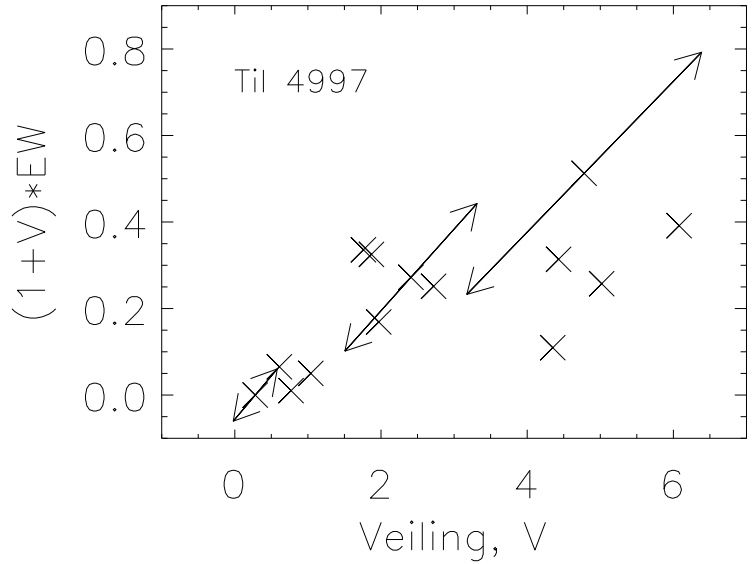
TiI 4997
(1+V)*EW
Veiling, V
0.0
0.2
0.4
0.6
0.8
0
2
4
6

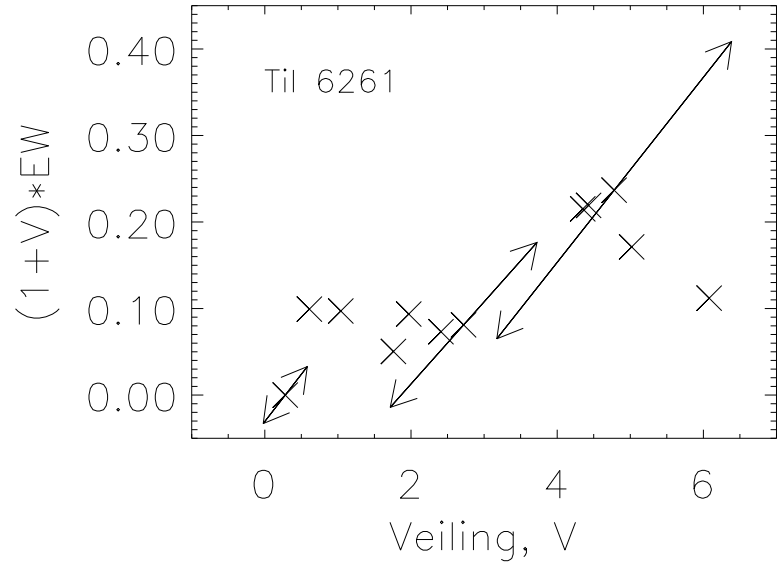
TiI 6261
(1+V)*EW
Veiling, V
0.00
0.10
0.20
0.30
0.40
0
2
4
6

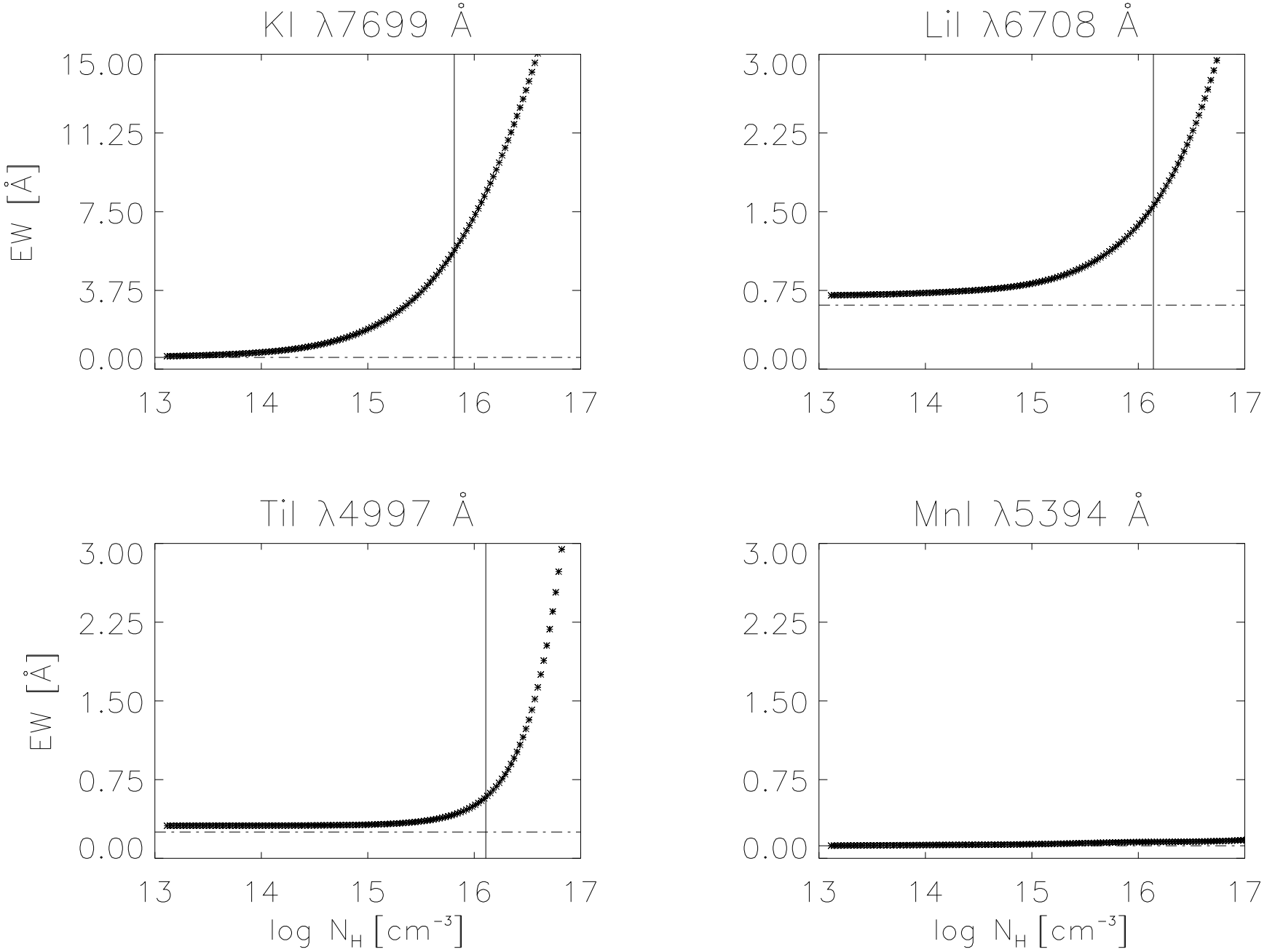
KI λ7699 Å
LiI λ6708 Å
TiI λ4997 Å
MnI λ5394 Å
EW [Å]
log N_H [cm^-3]
15.00
11.25
7.50
3.75
0.00
3.00
2.25
1.50
0.75
13
14
15
16
17

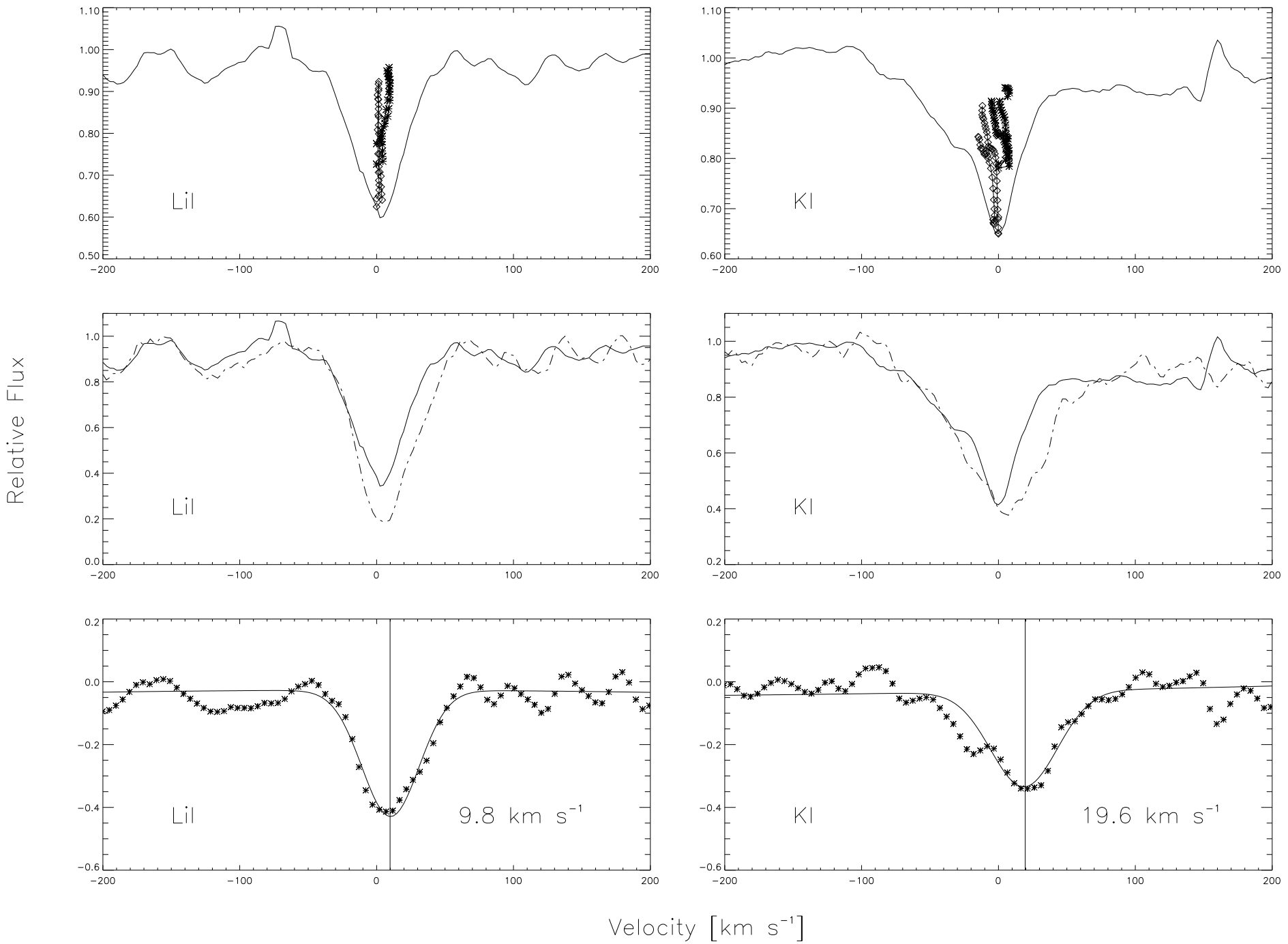
Li I
K I
Li I
K I
Li I
9.8 km s$^{-1}$
K I
19.6 km s$^{-1}$
Relative Flux
Velocity [km s$^{-1}$]